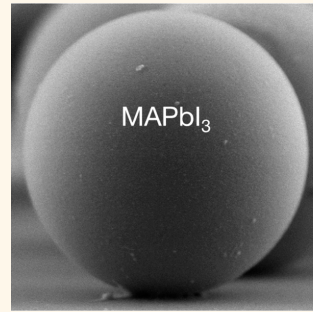


Conformal Organohalide Perovskites Enable Lasing on Spherical Resonators

Brandon R. Sutherland,[†] Sjoerd Hoogland,[†] Michael M. Adachi, Chris T. O. Wong, and Edward H. Sargent*

Department of Electrical and Computer Engineering, University of Toronto, 10 King's College Road, Toronto, Ontario M5S 3G4, Canada. [†]These authors (B.R.S. and S.H.) contributed equally.

ABSTRACT Conformal integration of semiconductor gain media is broadly important in on-chip optical communication technology. Here we deploy atomic layer deposition to create conformally deposited organohalide perovskites—an attractive semiconducting gain medium—with the goal of achieving coherent light emission on spherical optical cavities. We demonstrate the high quality of perovskite gain media fabricated with this method, achieving optical gain in the nanosecond pulse regime with a threshold for amplified spontaneous emission of $65 \pm 8 \mu\text{J cm}^{-2}$. Through variable stripe length measurements, we report a net modal gain of $125 \pm 22 \text{ cm}^{-1}$ and a gain bandwidth of $50 \pm 14 \text{ meV}$. Leveraging the high quality of the gain medium, we conformally coat silica microspheres with perovskite to form whispering gallery mode optical cavities and achieve lasing.



KEYWORDS: perovskites · atomic layer deposition · whispering gallery mode lasing · $\text{CH}_3\text{NH}_3\text{PbI}_3$

Rapid developments in thin-film organometallic perovskites are enabling high-efficiency and low-cost solar electricity devices.^{1–9} The excellent photophysical properties of this material¹⁰ have been further exploited toward light-emissive technology with reports of light-emitting diodes¹¹ and lasing from (i) bulk perovskite faceted crystals,¹² (ii) distributed feedback resonators,¹³ and (iii) planar whispering gallery cavities.¹⁴

We were motivated to explore whether lasing with spherical resonators could be achieved using perovskite active layers. This would require a continuous spherical coating of the perovskite film. Spherical resonators have yielded some of the highest confinement coefficients (*Q*-factors) among the full suite of optical cavities and have promising applications in on-chip integrated optical communications.^{15–17}

Unfortunately, we found that existing methods of perovskite film deposition from the solution phase or via directional coevaporation failed to produce, with the needed high consistency, the required conformal coverage of the curved resonator surfaces. For example, we attempted dip-coating in a liquid $\text{CH}_3\text{NH}_3\text{PbI}_3$ precursor and flash annealing but found that this approach did not produce consistent-thickness conformal layers of perovskite thin films on

the spheres and was sensitive to drying conditions.

To couple the perovskite gain material efficiently to spherical resonators, we would require a means of forming films that would provide intimate physical and hence optical coupling, minimize scattering loss, and form a conformal and even layer on the spheres. Techniques for conformal deposition of active materials are also important in materials science and optoelectronics broadly, such as for the direct integration of optical gain media with CMOS-defined cavities such as rib waveguides.

We developed a perovskite growth process which utilizes atomic layer deposition (ALD), a low-temperature and low-pressure thin-film formation method prized for its conformality, wide process window, and precise thickness control. We start from a film of ALD PbS, which forms the conformal seed layer. This film is then completely converted to PbI_2 via exposure to I_2 gas in a closed, nitrogen-inert, system. PbI_2 is subsequently converted to $\text{CH}_3\text{NH}_3\text{PbI}_3$ perovskite (MAPbI_3) through treatment with $\text{CH}_3\text{NH}_3\text{I}$ (complete description is available in the Methods section).

RESULTS AND DISCUSSION

Lasing relies on an active medium capable of sustaining population inversion and

* Address correspondence to ted.sargent@utoronto.ca.

Received for review August 28, 2014 and accepted October 14, 2014.

Published online October 14, 2014
10.1021/nn504856g

© 2014 American Chemical Society

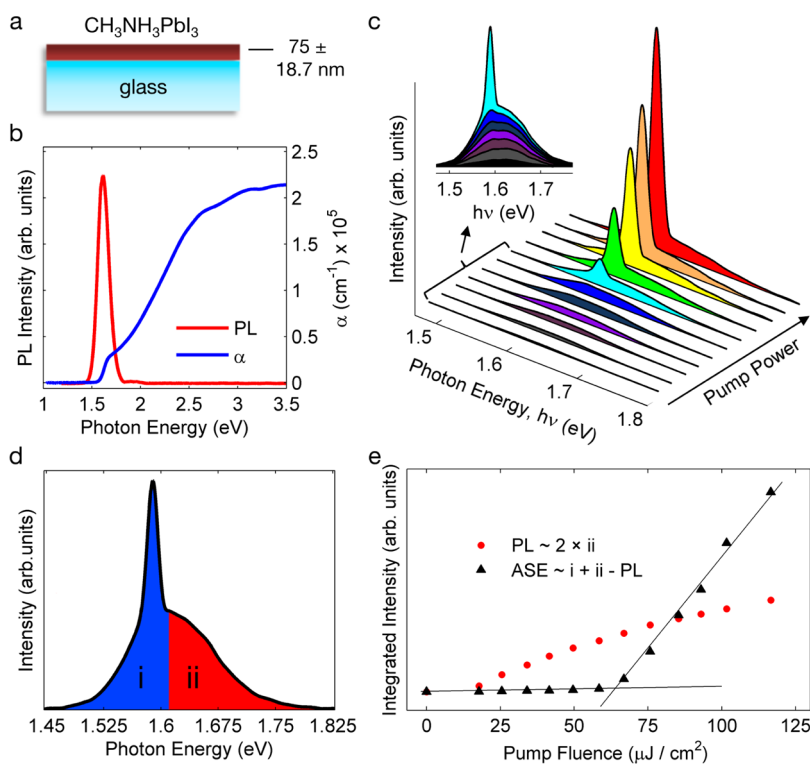


Figure 1. Amplified spontaneous emission from nanosecond pulsed excitation in $\text{CH}_3\text{NH}_3\text{PbI}_3$ grown via ALD. (a) MAPbI_3 (75 nm) is deposited onto a glass slide via perovskite-ALD. (b) Spectral absorption coefficient and photoluminescence under continuous-wave excitation. (c) Development of spectrally narrow amplified spontaneous emission with increasing pump power. (d) Emission spectra at $67 \mu\text{J cm}^{-2}$ of ASE coupled with PL. (e) Integrated emission intensity of PL and ASE as a function of pump fluence. A clear threshold for ASE is observed at $65 \pm 8 \mu\text{J cm}^{-2}$.

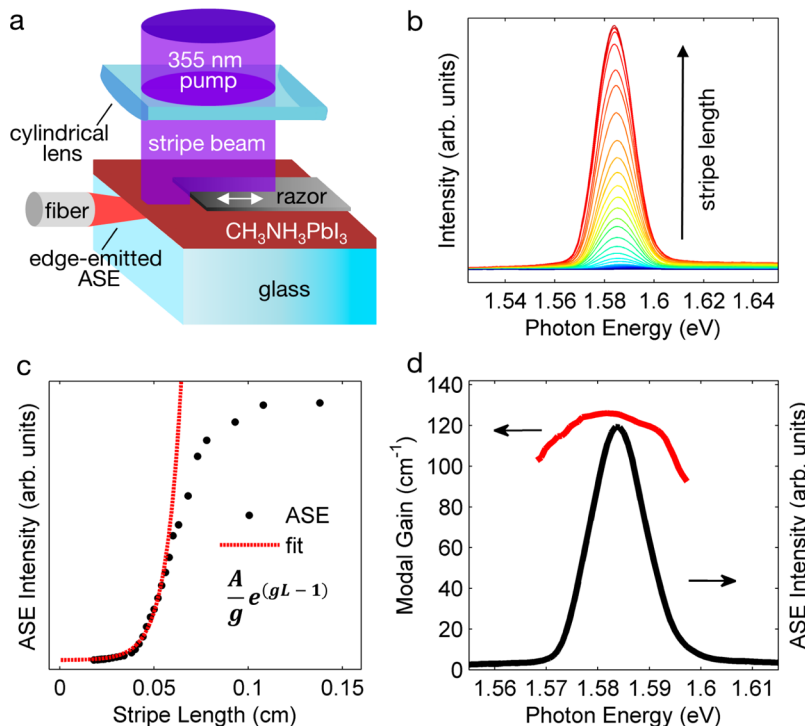


Figure 2. Net modal optical gain in $\text{CH}_3\text{NH}_3\text{PbI}_3$ ALD perovskites under nanosecond pulsed excitation. (a) Variable stripe length measurement setup for gain determination. (b) Emission spectra for increasing stripe length. (c) ASE intensity at an emission photon energy of 1.58 eV as a function of stripe length (black) and a linear amplifier fit (red) prior to the onset of gain saturation (see Methods for full details). (d) Spectral dependence of modal gain (red) and sample ASE spectrum at maximum stripe length (black). The peak gain bandwidth is $125 \pm 22 \text{ cm}^{-1}$, and the gain bandwidth is $50 \pm 14 \text{ meV}$.

optical gain through stimulated emission of radiation. We studied the optical properties of the perovskite active medium to elucidate the processes that govern lasing operation. All optical studies are performed at room temperature unless otherwise noted. We began by investigating the intensity-dependent spectral emission properties of a perovskite film on a lower-refractive-index substrate. We deposited a 75 ± 18.7 nm MAPbI_3 thin film via perovskite ALD onto a glass slide (Figure 1a) and confirmed that the film has an absorption onset at 1.55 eV with an absorption coefficient exceeding 10^4 cm^{-1} past the band edge (Figure 1b, blue), indicative of the direct band gap of the perovskite. Under 460 nm continuous-wave excitation, a broad photoluminescence (PL) signal centered at 1.61 eV with a full width at half-maximum (fwhm) of 130 meV (Figure 1b, red) is observed. The ultrasmall Stokes shift of 60 meV is indicative of a sharp band edge and minimal vibrational relaxation capable of sustaining optical gain close to the band edge.¹⁸ This increases the upper limit for the open-circuit voltage¹⁹ in perovskite photodiodes, consistent with the impressive values presented in published perovskite solar cells.

We subsequently excited the film using a pulsed laser source with an emission wavelength of 355 nm, pulse duration of 2 ns, and repetition rate of 100 Hz. Increasing the pump fluence reveals a threshold behavior at which the emission spectrum abruptly transitions from broad photoluminescence to a red-shifted narrow 17 meV line width emission peak centered at 1.58 eV (Figure 1c). The spectral narrowing for excitation above a threshold pump intensity is a signature of stimulated emission, here in the form of amplified spontaneous emission (ASE).

The resulting spectra contain superimposed emission from PL and ASE. To distinguish between these contributions, we estimate the emission due to PL by doubling the integrated intensity from the PL peak at 1.61 eV and above, averting the sharp ASE signature (Figure 1d, red). The total emission from ASE is then estimated as the total integrated intensity across the entire spectral range from 1.4 to 1.9 eV (Figure 1d, red + blue), minus the total PL intensity. Figure 1e shows the pump excitation dependence of the deconvolved PL and ASE emission. The integrated power that is emitted from the broad PL portion of the spectra follows a sublinear behavior (Figure 1e, red), indicative of state-filling near the conduction band edge. In contrast, the narrow spectral component exhibits a clear superlinear behavior with a threshold energy density of $65 \pm 8 \mu\text{J cm}^{-2}$ (Figure 1e, black). This threshold behavior with excitation intensity is another characteristic of stimulated emission, signaling that population inversion has been achieved.

The capability of perovskites to demonstrate stimulated emission in the nanosecond pulse excitation

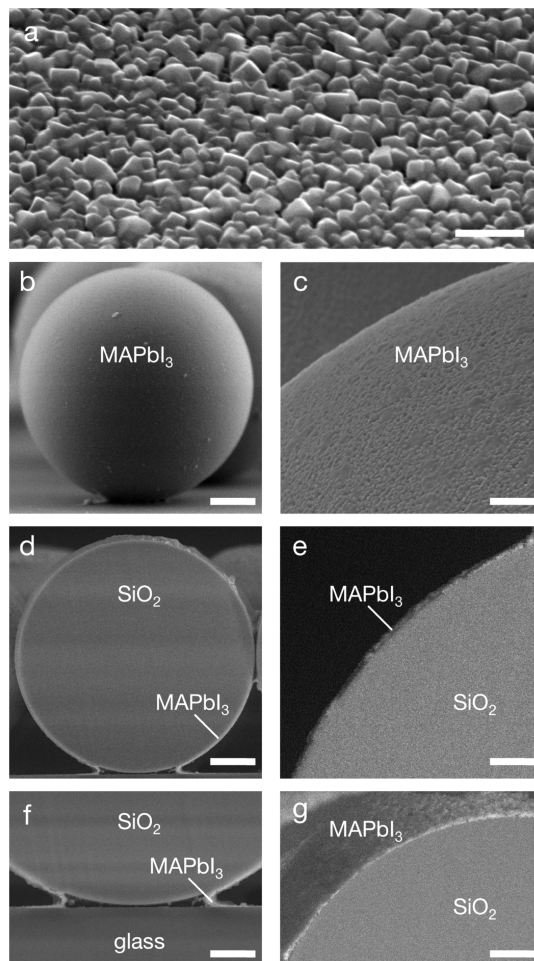


Figure 3. Scanning electron microscope images of microspheres coated via perovskite ALD. (a) Image of the 45° perovskite surface. (b) Zoomed-out image of the entire microsphere coated with perovskite. (c) Zoomed-in image showing coverage all along the curved surface of the sphere. (d) Cross-sectional image of a sphere cut down the center with focused ion beam milling revealing a uniform coating around the circumference of the sphere. (e) Zoomed-in image on a cross section of the sphere, showing distinct perovskite and SiO_2 regions. (f) Zoomed-in image of sphere–substrate interface, showing a continuous film with good infiltration into the grooves. (g) Angled zoomed-in image of the sphere's cross section, showing a good uniform coating of perovskite around the surface of the sphere. Scale bars: (a–g) 0.2, 10, 2, 10, 3, 5, 4 μm .

regime, orders of magnitude longer than previous reports,^{12–14} is a strong indication of a high-quality gain medium. The absorption coefficient at the spectral position of the ASE signal is evaluated to be $3100 \pm 830 \text{ cm}^{-1}$. This value is similar to well-developed, single-crystal semiconductors such as GaAs,²⁰ a key performance attribute that suggests promise for thin-film perovskites for optical amplification. We also investigated the perovskite gain medium under continuous-wave, millisecond, and microsecond pulse durations and found that emission intensity nonlinearity and spectral narrowing characteristics of amplified spontaneous emission were not observed. This is a result of the ASE threshold lying above the

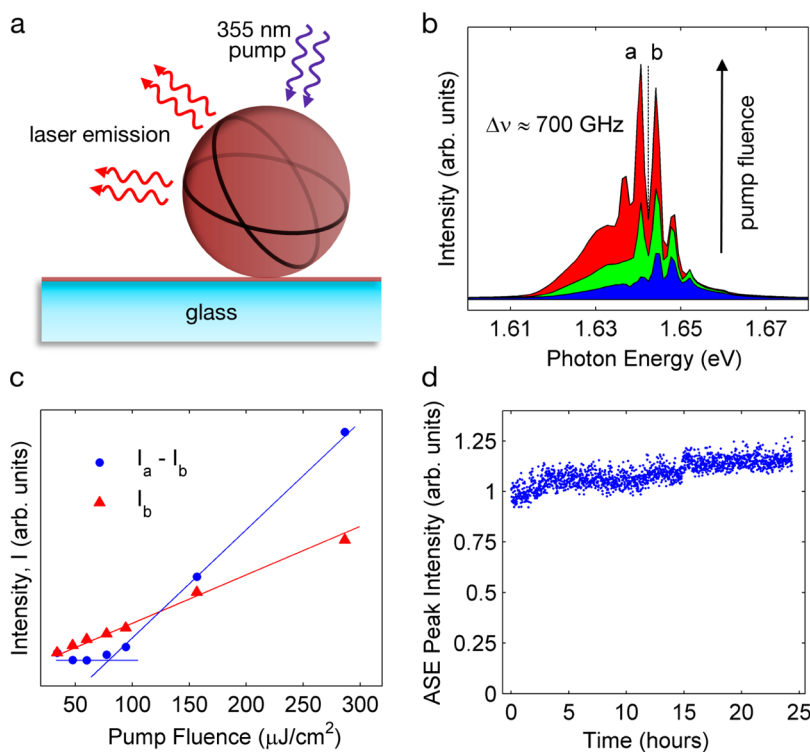


Figure 4. Modal confinement and lasing in perovskite-coated silica microspheres. (a) Schematic showing a perovskite-coated microsphere absorbing pump light and coupling luminescence into the cavity, resulting in laser emission. (b) Spectral dependence of perovskite-coated microsphere emission on pump power at $T = 80\text{ K}$ for three different pump fluences ($100\text{ }\mu\text{J cm}^{-2}$, blue; $175\text{ }\mu\text{J cm}^{-2}$, green; and $300\text{ }\mu\text{J cm}^{-2}$, red). Distinct laser modes are observed with a free spectral range of 700 GHz . (c) Lasing emission intensity dependence on pump fluence. The intensity of the dominant lasing peak at 1.642 eV , “a”, with the adjacent background signal at “b” subtracted is compared to the background signal. The slope efficiency of the lasing mode (blue) is greater than that of the background (red), and a lasing threshold is observed at a pump fluence of $75 \pm 11\text{ }\mu\text{J cm}^{-2}$. (d) Twenty-four hour ASE stability under lasing conditions.

damage threshold of the film under these conditions. Strategies that reduce the modal losses and efficiently convey heat from the perovskite thin film could facilitate progress toward achieving population inversion under these pulse durations.

The pronounced threshold as a function of excitation intensity, from photoluminescence alone to the clear emergence of narrow-band amplified spontaneous emission, indicates optical gain with a gain relaxation time that is shorter than the carrier buildup time.²¹ We investigated the net modal optical gain in the perovskite medium using the variable stripe length characterization technique.²² Here, we excite our sample at a fixed pump fluence of $150\text{ }\mu\text{J cm}^{-2}$, above the threshold for ASE. We focus the circular pump beam to a stripe using a cylindrical lens. An adjustable straight-edge razor blade placed close to the sample controls the length of the excitation stripe, and the emission is collected from a cleaved edge of the sample using an optical fiber (Figure 2a).

We examine the dependence of the edge-emission intensity of a stripe-pumped perovskite above the ASE threshold on the length of the excitation beam. The full spectrum for all stripe lengths is shown in Figure 2b. The emission intensity at 1.58 eV , the energy at which the ASE signal is maximum, exhibits an exponential

behavior as a function of increasing stripe length prior to gain saturation. For increased stripe lengths, gain saturation occurs in regions in which free carriers have been depleted by ASE.²³ An exponential fit of the collected emission in the small stripe regime (stripe length $<0.535\text{ cm}$) with a 1D amplifier model yields an estimated gain value of $125 \pm 22\text{ cm}^{-1}$ (Figure 2d,e). This gain value corresponds to the modal gain, which combines the subunity confinement of the optical mode to the gain medium, multiplied by the material gain, and reduced by the effect of modal waveguide losses. This value for the net modal gain for a 2 ns pump pulse duration is comparable to prior reports on organohalide perovskites under 150 fs pulse durations.¹² It is also comparable to the net modal gain in other non-single-crystal semiconducting systems such as colloidal quantum dots,^{24–27} silicon nanocrystals,²⁸ and semiconducting polymers.²⁹ The spectrally resolved modal gain bandwidth is $50 \pm 14\text{ meV}$, obtained from analysis of ASE signal versus stripe length at each wavelength. Gain bandwidths of this magnitude are similar to those found in compound semiconductors,²⁰ consistent with the sharp band edge of perovskites, remarkable considering the perovskite films’ polycrystalline nature.

The presence of net optical gain, with a demonstration of ASE, highlights the potential for ALD perovskites

to serve as active materials for lasing under nanosecond pulsed excitation. We formed the gain medium using perovskite ALD onto an optical resonator of 52 μm diameter silica microspheres. Lasing can be achieved provided the cavity losses are less than the modal gain; thus only if the microspheres were conformally coated would it be possible to achieve efficient waveguiding and therefore a net positive modal gain in the film that coated the sphere.

To study the perovskite growth, we imaged the coated microspheres with scanning electron microscopy (SEM). Figure 3a shows a 45° tilt SEM image of the perovskite surface, revealing structured polycrystalline domains. Figure 3b,c shows the perovskite coating onto the curved surface of the microsphere. Using focused ion beam (FIB) milling, we cut the spheres in half down the center to better study the film formation and coverage. Figure 3d–g reveals a uniform, continuous coating of perovskite covering the surface of the sphere with infiltration deep into the trenches near the sphere–substrate interface, something not readily achievable using traditional deposition methods.

We subsequently optically pumped the perovskite-coated microspheres and measured the emission spectra. We expect whispering gallery modes to couple into the sphere and produce optical feedback *via* various pathways along the circumference of the cavity, resulting in multidirectional lasing (Figure 4a). Figure 4b shows the emission spectra of perovskite-coated microspheres at $T = 80$ K at varying excitation levels. This spectrum exhibits clearly defined modes with a regular spacing of 3 meV, corresponding to an effective refractive index of approximately 1.4, indicating that

the mode is predominantly confined to the silica perovskite region. Figure 4c shows the dependence of emission intensity on pump fluence. The background signal is subtracted from the adjacent cavity mode at 1.642 eV, and the dependence of intensity on pump fluence is plotted against the background. A clear threshold is observed for the cavity mode at a pump fluence of $75 \pm 11 \mu\text{J cm}^{-2}$. Further, the slope efficiency of the cavity mode signal is greater than that of the background. We attribute this threshold behavior of intensity and spectral features to lasing cavity modes, and we demonstrate that the perovskite gain medium is stable under these conditions for 24 h (Figure 4d). The spectral bandwidth of the laser modes are dominantly limited by the resolution of the collection optics, thus we conservatively estimate the lower bound of the Q-factor for these resonators to be on the order of 10^3 .

CONCLUSIONS

The results presented herein show that ALD perovskites offer conformal deposition onto substrates of various curvatures and aspect ratios. This fabrication strategy forms perovskite films with excellent lasing-relevant optical properties, enabling them to sustain population inversion when excited using low peak intensity pumping, and with excellent material properties, allowing ready formation of conformal waveguiding films when deposited on spherical resonators. Facile conformal deposition of perovskite light emitters has the potential to enable applications such as low-cost on-chip optical communication systems readily integrated with silicon photonics technology.

METHODS

ALD Perovskite Sample Fabrication. Glass substrates were prepared by first sonication in acetone, then isopropyl alcohol and then deionized water, each for 15 min. Samples to be used for lasing studies employed silica spheres (52 μm diameter, suspended in water) dispensed onto the surface of the glass. Excess water was dried by heating on a hot plate at 120 °C for 1 min. Samples were exposed to a 10 min 100 mTorr oxygen plasma treatment immediately prior to atomic layer deposition.

$\text{CH}_3\text{NH}_3\text{PbI}_3$ perovskite films were fabricated on these substrates by a three-step method. (A) PbS deposition: Cleaned glass slides were placed into a Cambridge Savannah S100 atomic layer deposition system with the sample chamber held at 150 °C. Alternating pulses of $\text{Pb}(\text{tmhd})_2$ and H_2S precursors (0.5 s pulse duration for both) built up the PbS film of a desired thickness. The purge time between precursor pulses was 20 s, and a nitrogen carrier gas was used at a volumetric flow rate of 10 sccm. (B) PbI_2 conversion: Iodine chips (100 mg) were placed into a 250 mL nitrogen-sealed container which contains the PbS films. The container was heated on a 120 °C hot plate for 16 h. After treatment, the samples were completely yellow and were converted to PbI_2 . (C) MAPbI_3 conversion: The PbI_2 films were dipped into a 30 mg/mL solution of $\text{CH}_3\text{NH}_3\text{I}$ dissolved in isopropyl alcohol (IPA) for 60 s, immediately dipped into IPA for another 60 s, and then dried on a hot plate at 70 °C for 30 min.

Focused Ion Beam and Scanning Electron Microscopy. A Hitachi table-top ion mill model IM 4000 was used for sample FIB

preparation. Argon ions were used at an accelerating voltage of 6 kV and a discharge voltage of 1.5 kV. The sample was milled for 3.5 h with the glass substrate facing the ion source to allow for gentler milling. Samples were imaged with a Hitachi NB-5000 high-resolution CFESEM. An accelerating voltage of 20 kV and a variable pressure of 60 Pa were used and imaged using a highly sensitive ultravariable pressure detector.

Optical Excitation and Collection. Unless otherwise noted, samples were optically excited using a 355 nm frequency-tripled Nd: YAG laser with a pulse width of 2 ns and a repetition rate of 100 Hz. All spectral data were collected using an Ocean Optics USB2000+ UV-vis spectrometer without an input aperture, with the spectral resolution defined by the width of the input fiber core. A 62.5 μm core diameter fiber was used to collect all spectra, except for the data presented in Figure 4b,c, which were collected with a single mode fiber, with the SMF case producing a spectral resolution of ~0.4 nm, enabling us to distinguish individual laser modes. To detect whispering gallery lasing modes, we focused the pump beam to a circular spot so that it illuminated a cluster of four spheres as well as some of the planar background. All measurements of laser power were taken using an Ophir Laserstar 1Z01600 single-channel digital power meter.

Absorption Coefficient. The optical density, A_{OD} , of the perovskite film was measured using a PerkinElmer Lambda 950 spectrophotometer with an integrating sphere. A DekTak 3 profilometer was used to measure the film thickness, d .

This was used to calculate the absorption coefficient, $\alpha = \log_{10}(e) \times A_{OD}/d$.

Variable Stripe Length Measurement. The variable stripe length technique was employed to determine optical gain in the $\text{CH}_3\text{NH}_3\text{PbI}_3$ film. Intensity at each wavelength as a function of stripe position was fit to a linear amplifier model: $I_{ASE}(L) = A(e^{gL} - 1)/g$, where I_{ASE} is the intensity of the ASE, L is the stripe length, g is the modal gain to be determined, and A is a pre-exponential factor related to the ratio of emitted spontaneous emission to modal gain.²³

Conflict of Interest: The authors declare no competing financial interest.

Acknowledgment. This publication is based in part on work supported by an award (KUS-11-009-21) from the King Abdullah University of Science and Technology (KAUST), by the Ontario Research Fund Research Excellence Program and by the Natural Sciences and Engineering Research Council (NSERC) of Canada. The authors thank S. Boccia for FIB and SEM imaging of ALD perovskite-coated microspheres, and S.-R. Jean for help with figure art.

REFERENCES AND NOTES

- Im, J.-H.; Lee, C.-R.; Lee, J.-W.; Park, S.-W.; Park, N.-G. 6.5% Efficient Perovskite Quantum-Dot-Sensitized Solar Cell. *Nanoscale* **2011**, *3*, 4088.
- Kim, H.-S.; Lee, C.-R.; Im, J.-H.; Lee, K.-B.; Moehl, T.; Marchioro, A.; Moon, S.-J.; Humphry-Baker, R.; Yum, J.-H.; Moser, J. E.; et al. Lead Iodide Perovskite Sensitized All-Solid-State Submicron Thin Film Mesoscopic Solar Cell with Efficiency Exceeding 9%. *Sci. Rep.* **2012**, *2*.
- Lee, M. M.; Teuscher, J.; Miyasaka, T.; Murakami, T. N.; Snaith, H. J. Efficient Hybrid Solar Cells Based on Mesosuperstructured Organometal Halide Perovskites. *Science* **2012**, *338*, 643–647.
- Noh, J. H.; Im, S. H.; Heo, J. H.; Mandal, T. N.; Seok, S. I. Chemical Management for Colorful, Efficient, and Stable Inorganic–Organic Hybrid Nanostructured Solar Cells. *Nano Lett.* **2013**, *13*, 1764–1769.
- Heo, J. H.; Im, S. H.; Noh, J. H.; Mandal, T. N.; Lim, C.-S.; Chang, J. A.; Lee, Y. H.; Kim, H.; Sarkar, A.; Nazeeruddin, M. K.; et al. Efficient Inorganic–Organic Hybrid Heterojunction Solar Cells Containing Perovskite Compound and Polymeric Hole Conductors. *Nat. Photonics* **2013**, *7*, 486–491.
- Burschka, J.; Pellet, N.; Moon, S.-J.; Humphry-Baker, R.; Gao, P.; Nazeeruddin, M. K.; Grätzel, M. Sequential Deposition as a Route to High-Performance Perovskite-Sensitized Solar Cells. *Nature* **2013**, *499*, 316–319.
- Liu, M.; Johnston, M. B.; Snaith, H. J. Efficient Planar Heterojunction Perovskite Solar Cells by Vapour Deposition. *Nature* **2013**, *501*, 395–398.
- Jeon, N. J.; Noh, J. H.; Kim, Y. C.; Yang, W. S.; Ryu, S.; Seok, S. I. Solvent Engineering for High-Performance Inorganic–Organic Hybrid Perovskite Solar Cells. *Nat. Mater.* **2014**, *13*, 897–903.
- Green, M. A.; Ho-Baillie, A.; Snaith, H. J. The Emergence of Perovskite Solar Cells. *Nat. Photonics* **2014**, *8*, 506–514.
- Stoumpos, C. C.; Malliakas, C. D.; Kanatzidis, M. G. Semiconducting Tin and Lead Iodide Perovskites with Organic Cations: Phase Transitions, High Mobilities, and Near-Infrared Photoluminescent Properties. *Inorg. Chem.* **2013**, *52*, 9019–9038.
- Tan, Z.-K.; Moghaddam, R. S.; Lai, M. L.; Docampo, P.; Higler, R.; Deschler, F.; Price, M.; Sadhanala, A.; Pazos, L. M.; Credgington, D.; et al. Bright Light-Emitting Diodes Based on Organometal Halide Perovskite. *Nat. Nanotechnol.* **2014**, *9*, 687–692.
- Xing, G.; Mathews, N.; Lim, S. S.; Yantara, N.; Liu, X.; Sabba, D.; Grätzel, M.; Mhaisalkar, S.; Sum, T. C. Low-Temperature Solution-Processed Wavelength-Tunable Perovskites for Lasing. *Nat. Mater.* **2014**, *13*, 476–480.
- Deschler, F.; Price, M.; Pathak, S.; Klintberg, L. E.; Jarausch, D.-D.; Higler, R.; Hüttner, S.; Leijtens, T.; Stranks, S. D.; Snaith, H. J.; et al. High Photoluminescence Efficiency and Optically Pumped Lasing in Solution-Processed Mixed Halide Perovskite Semiconductors. *J. Phys. Chem. Lett.* **2014**, *5*, 1421–1426.
- Zhang, Q.; Ha, S. T.; Liu, X.; Sum, T. C.; Xiong, Q. Room-Temperature Near-Infrared High-Q Perovskite Whispering-Gallery Planar Lasers. *Nano Lett.* **2014**, *14*, 5995–6001.
- Vernooij, D. W.; Ilchenko, V. S.; Mabuchi, H.; Streed, E. W.; Kimble, H. J. High-Q Measurements of Fused-Silica Microspheres in the Near Infrared. *Opt. Lett.* **1998**, *23*, 247–249.
- Cai, M.; Painter, O.; Vahala, K. J. Observation of Critical Coupling in a Fiber Taper to a Silica-Microsphere Whispering-Gallery Mode System. *Phys. Rev. Lett.* **2000**, *85*, 74.
- Kalkman, J.; Polman, A.; Kippenberg, T. J.; Vahala, K. J.; Brongersma, M. L. Erbium-Implanted Silica Microsphere Laser. *Nucl. Instrum. Methods Phys. Res., Sect. B* **2006**, *242*, 182–185.
- Stranks, S. D.; Eperon, G. E.; Grancini, G.; Menelaou, C.; Alcocer, M. J. P.; Leijtens, T.; Herz, L. M.; Petrozza, A.; Snaith, H. J. Electron–Hole Diffusion Lengths Exceeding 1 Micrometer in an Organometal Trihalide Perovskite Absorber. *Science* **2013**, *342*, 341–344.
- Guyot-Sionnest, P. Electrical Transport in Colloidal Quantum Dot Films. *J. Phys. Chem. Lett.* **2012**, *3*, 1169–1175.
- Fermann, M.; Galvanauskas, A.; Sucha, G. *Ultrafast Lasers: Technology and Applications*, 1st ed.; CRC Press: Boca Raton, FL, 2002.
- Klimov, V. I. Optical Gain and Stimulated Emission in Nanocrystal Quantum Dots. *Science* **2000**, *290*, 314–317.
- Shaklee, K. L. Direct Determination of Optical Gain in Semiconductor Crystals. *Appl. Phys. Lett.* **1971**, *18*, 475.
- Negro, L. D.; Bettotti, P.; Cazzanelli, M.; Pacifici, D.; Pavesi, L. Applicability Conditions and Experimental Analysis of the Variable Stripe Length Method for Gain Measurements. *Opt. Commun.* **2004**, *229*, 337–348.
- Malko, A. V.; Mikhailovsky, A. A.; Petruska, M. A.; Hollingsworth, J. A.; Htoon, H.; Bawendi, M. G.; Klimov, V. I. From Amplified Spontaneous Emission to Microring Lasing Using Nanocrystal Quantum Dot Solids. *Appl. Phys. Lett.* **2002**, *81*, 1303.
- Petruska, M. A.; Malko, A. V.; Voyles, P. M.; Klimov, V. I. High-Performance, Quantum Dot Nanocomposites for Nonlinear Optical and Optical Gain Applications. *Adv. Mater.* **2003**, *15*, 610–613.
- Dang, C.; Lee, J.; Breen, C.; Steckel, J. S.; Coe-Sullivan, S.; Nurmi, A. Red, Green and Blue Lasing Enabled by Single-Exciton Gain in Colloidal Quantum Dot Films. *Nat. Nanotechnol.* **2012**, *7*, 335–339.
- Hoogland, S.; Sukhovatkin, V.; Howard, I.; Cauchi, S.; Levina, L.; Sargent, E. H. A Solution-Processed 1.53 μm Quantum Dot Laser with Temperature-Invariant Emission Wavelength. *Opt. Express* **2006**, *14*, 3273–3281.
- Pavesi, L.; Dal Negro, L.; Mazzoleni, C.; Franzo, G.; Priolo, F. Optical Gain in Silicon Nanocrystals. *Nature* **2000**, *408*, 440–444.
- Laquai, F.; Mishra, A. K.; Müllen, K.; Friend, R. H. Amplified Spontaneous Emission of Poly(ladder-type phenylene): The Influence of Photophysical Properties on ASE Thresholds. *Adv. Funct. Mater.* **2008**, *18*, 3265–3275.